PERGAMON

Deep-Sea Research I 47 (2000) 1881–1897

DEEP-SEA RESEARCH
PART I

Sediment erosion thresholds and characteristics of resuspended aggregates on the western European continental margin

Laurenz Thomsen[a,*], Giselher Gust[b]

[a]*GEOMAR, Kiel, G. University of Washington School of Oceanography, Campus Box 357940, Seattle, WA 98195-7940, USA*

[b]*Technical University Hamburg-Harburg, G. University of Washington School of Oceanography, Campus Box 357940 Seattle, WA 98195-7940, USA*

Received 20 May 1999; received in revised form 20 July 1999; accepted 23 November 1999

Abstract

Sediment erosion thresholds and characteristics of resuspended aggregates were experimentally determined on cores from the western European continental margin with a ship-borne erosion chamber augmented by image analysis. Bottom sediments (212–4940 m water depth) had a thin surface layer that was resuspended as aggregates (median diameter 125–2403 μm) under critical shear velocities (u_{*c}) of 0.4–1.2 cm s^{-1}. For the underlying sediments, eroded as primary particles, u_{*c} increased with water depth from 0.7 cm s^{-1} (sandy shelf sediments) to 2.1 cm s^{-1} (lower slope sediments). A two-layer concept of the sediment interface is discussed which distinguishes between an underlying sediment layer, bound by both physico-chemical and biological adhesion and a more easily resuspendable surface aggregate layer. The surface layer consists mainly of aggregates in the 140–450 μm size range and is resuspended at mean thresholds u_{*c} of 0.8–0.9 cm s^{-1}. These aggregates can subsequently be transported in tide-related resuspension–deposition loops over long distances.

Keywords: Critical shear velocity; Continental margin; Aggregate resuspension

* Corresponding author. Present address: School of Oceanography, University of Washington, Campus Box 357940, Seattle, WA 98195-9940, USA. Tel.: + 1-206-543-7615.

E-mail address: gust@tu-harburg.de, lthomsen@geomar.de (L. Thomsen).

0967-0637/00/$ - see front matter
PII: S0967-0637(00)00003-0

1. Introduction

Ocean margins and continental slope regimes are natural boundaries common to oceanic and shelf sea domains. They are areas of enhanced productivity, and biologically mediated downslope transport of particles may be large, exhibiting strong links between the two realms. Recent research at different continental margins revealed that, in order to explain benthic carbon remineralization rates, in addition to the vertical export flux of organic particles from the sea surface as measured by sediment traps, lateral advection of particulate matter has to be considered as well (Jahnke et al., 1990; Biscaye et al., 1994; Graf et al., 1995; Thomsen, 1998). At present, estimates of shelf export of phytoplankton production to slope and abyssal depths are not well known and vary remarkably from 1–10% to about 90% (Walsh et al., 1981; Biscaye et al., 1994).

Lateral transport of particulate matter is driven largely by hydrodynamics within the benthic boundary layer (BBL), initiating and controlling the particle exchange between sediments of the sea floor and the water column (McCave, 1986; Dickson and McCave, 1986; Thorpe and White, 1988). Detailed observations of hydrodynamical, biological and sedimentological BBL characteristics of continental margins are extremely rare. Most studies indicate that the quality and quantity of deposited organic matter is strongly influenced by decomposition processes during the flow-controlled processes of sedimentation, lateral sediment transport and resuspension (Auffret et al., 1994) in addition to microbial and faunal activity at the sediment–water interface and in the surface sediments (Graf et al., 1995; Thomsen et al., 1995; Ritzrau, 1996). Well-sorted, abiotic fine-bed sediments respond as non-cohesive particles down to about 10 μm diameter to the acting bottom stress; Shields-type diagrams then provide the links between flow, bed stability/behaviour and transport mode. Below this size, particles bond electrochemically and become cohesive, either as clay minerals with their charge imbalances entering the composition spectrum (McCave et al., 1995) or as particles (such as quartz or debris) with size-dependent surface forces.

Cohesive sediments with biological interaction, found at mid- and lower-slope regions of continental margins, are part of a complex chain of events which are not fully understood in their relation to bed stability, flow structure, material fluxes, and ecosystem dynamics. For example, the latest studies on transport pathways in the benthic boundary layers of continental margins reveal that major particle transport occurs as a low-concentration suspension in the lowest few decimetres above the sea floor. It is not clear to date to what extent at typical tidal flow speeds the primary particles (Middleton and Southard, 1984) of the sea floor sediments are involved in addition to the particles torn off the bed as aggregates (Thomsen and van Weering, 1998; Thomsen, 1998).

To understand and quantify these transport processes, both laboratory and field studies are required to link hydrodynamics with aggregate and bed formation. Advective near-bed fluid flow imports both particles and solutes from sources upstream (in addition to those arriving from above) that can serve as food (and fuel) for benthic communities. Through the coupling to the local ecosystem (the benthic mill),

more or less nutrient-rich, reprocessed or remoulded particles, such as faecal wastes or detritus, and dissolved metabolites are subsequently exported (moved downstream) after resuspension. For models as well as calculations of the mass fluxes associated with this bed-flow-biology interaction, several important particle and hydrodynamic parameters need to be determined: the bottom stress (τ), expressed as friction velocity (u_*), the turbulence intensities and the mean local horizontal flow speed together with the controlling variables of sediment transport: the critical erosion stress (τ_c), the critical deposition stress (τ_d), and the particle settling velocity (w_s) (Middleton and Southard, 1984). In order to obtain τ_c, erosion devices have to be used (Tsai and Lick, 1986; Gust and Müller, 1997).

The goal of this study was to determine at different transects and water depths of the western European continental margin the sea bed erodibility, especially when significant biological interaction was expected. In particular, we wanted to investigate if the sediments at the continental margin consisted of a homogenized sediment with an easily predictable threshold behaviour and the extent to which biostabilization or destabilization is discernible for these sediments. A concept of the benthic mass transport of probably universal nature with strong interdisciplinary links between flow, sediment, and biology and relevant ecological consequences emerges from the results.

2. Methods

Sediments were collected during five cruises to the European continental margins the Celtic Sea between 45° and 55°N, 5° and 25°W, in the months of July 1995, August 1996, May 1997, August 1997 and August 1998 (Fig. 1). Cores were taken with a boxcorer built by the Netherlands Institute for Sea Research (NIOZ). It utilizes cylindrical samplers of 50 cm diameter, with closing lids on the core tops to retain the top-layer sediments at the water interface as undisturbed as possible (van Weering et al., 1998). For the determination of the critical erosion stress τ_c ($N\,m^{-2} = Pa$) $= u_{*c}^2 \rho$ (where u_{*c} is the critical friction velocity ($m\,s^{-1}$) and ρ is the fluid density ($kg\,m^{-3}$), subcores of 20 cm diameter were taken from the box corers and stored under in situ temperatures. Critical erosion stress was obtained onboard in an erosion chamber with controlled bottom stress (Gust and Müller, 1997), into which the 20 cm subcore and in situ seawater at field temperatures (overlying water height 10 cm, Fig. 2a) were inserted. Calibration of the bottom stress of the erosion chamber was done by a variety of approaches. They included use of calibrated skin friction probes (Gust, 1988) placed at radial positions with $\Delta r = 2\ cm$ at the interface similar to the protocol used by Buchholtz et al. (1989) use of the alabaster dissolution technique (Opdyke et al., 1987), application of 1-d and 2-d Laser-Doppler-Anemometry (LDA) in appropriate orientations measuring the 3-d flow field inside the chamber, and use of LDA and boundary-layer hot film probes (TSI, model 1218 NACl) to determine the velocity gradient in the viscous sublayer. Data were thus collected for chamber diameters ranging from 10 to 40 cm, which formed the basis for a semi-analytical hydrodynamical model of the interfacial stress pattern, verified at an accuracy $\leqslant 5\%$ for the

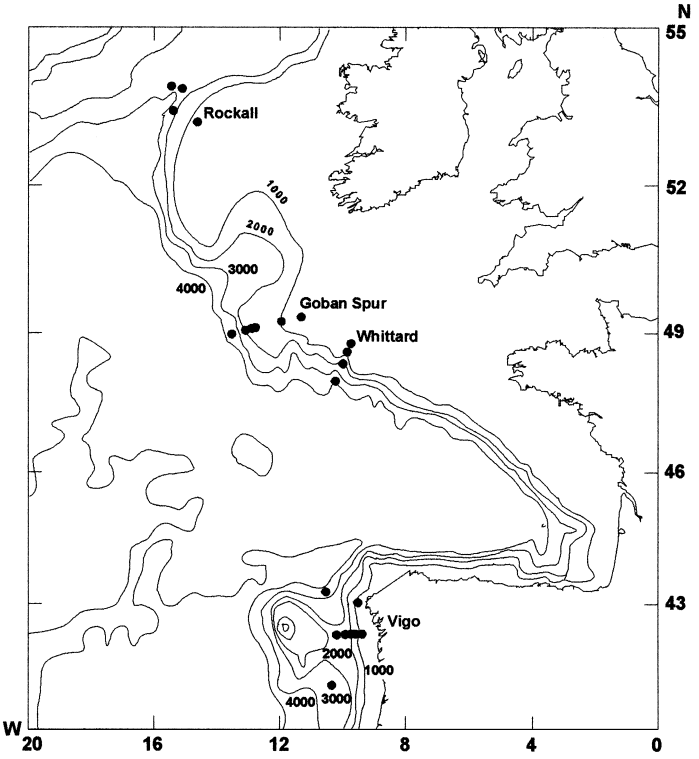

Fig. 1. Location of the study sites where investigations on sediment erosion thresholds and aggregate characteristics were carried out between 1995 and 1997.

spatially averaged bottom stress τ. Unexpectedly, the model revealed a temperature dependency of the bottom stress distribution which is controlled by the strength of the angular flow (and thus the chamber diameter). This result was subsequently verified experimentally and applies to all chambers with rotating flows. Furthermore, the chamber bottom stress pattern was independently verified in intercalibration experiments of existing respiration chambers within the EU-program ALIPOR (Priede, 1999). Interfacial threshold and flux data of solutes (Booij et al., 1994), pigments (Wiltshire et al., 1997), and particles (Gust and Müller, 1997) have been determined, among others, with this chamber, whose accuracy in bottom stress magnitude for hydrodynamically smooth surfaces lies at similar levels as that obtainable by fully developed flume boundary layer flows. Repeatability and stable operation have been demonstrated by determining, for example, the standard deviation of sediment entrainment rates at values $\leqslant 50\%$ of the mean for both cohesive sediments (5 replicates per data point) and in sand/clay mixtures (up to 10 replicates per data point) of cores that had strictly followed the same core preparation protocol and were eroded at the same pre-selected settings for the chamber bottom stress. The spatial and temporal distribution of the wall shear stress is controlled in the chamber by setting

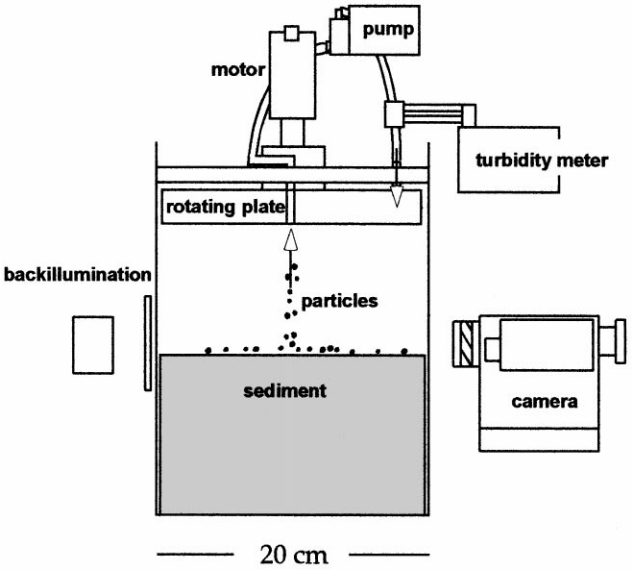

Fig. 2. Schematic drawing of the microcosm for sediment resuspension experiments. The initial bedload is concentrated during erosion over the enclosed area in the centre of the chamber and thus the camera and the turbidity meter detect very small amounts of particles.

simultaneously the rotation rate of a stirring disk placed 8.0 ± 0.3 cm above the water–sediment interface, and the volume flow rate of recirculated sea water removed through the rotating centre shaft. In the chamber, the particles are eroded at their location by the acting bottom stress (which is homogeneous over the sediment surface within an error margin $< 5\%$ by the same physical forces acting on the sediment surface as in other erosion devices operating by tangential forces). The novelty of this device lies in the fact that in contrast to a linear flume, where the bottom stress vector points on average in the downstream direction, the stress vector constitutes logarithmic spirals towards the centre of the chamber. The eroded particles thus follow a centre-directed path with a tangential and a radial component. In the centre, the particles move upward in the vortex due to the central fluid removal as part of the recirculation process. No mixing with the overlying fluid occurs during the very first transport of particles towards the centre. The eroded particles are mixed into the water column at the outlet of the return path.

Experiments were run on the research vessel during times of calm seas on a table with hydraulic vibration absorber under in-situ temperature conditions of 2–10°C. With the selected erosion/respiration chamber it was possible incrementally to increase the spatially homogeneous bottom stress in the range $0.005 < \tau < 0.5$ N m^{-2}, of which as minimum value $\tau = 0.01$ N m^{-2} was chosen, and stepwise increases τ of 0.001 N m^{-2}. Each step of constant stress exposure lasted for a minimum of 10 min. Onset of particle erosion and of sediment erosion for the disaggregated fine sediment

fraction (<100 μm diameter) was determined by a calibrated NTU turbidity meter (Nephelometric Turbidity Units, Model 800, Engineered Systems & Design, USA, 0 to 19.99 NTU range, resolution of 0.1%, onset on 10% increase). Data on turbidity were recorded every 10 min, and water samples for size analyses were taken, after sediment erosion had started. The size distribution and mean diameter of these samples were analysed with a Coulter counter (Type Multisizer), and the sediment size/weight distribution was determined by the modified Atterberg method (Blaume, 1992). Onset of sediment erosion for the aggregated fraction (>100 μm diameter and named 100^{+}aggregates) was determined by a particle camera with 20-fold magnification (Thomsen et al., 1996), focussed on the water layers immediately above the sediment (Fig. 2). With an additional no.3 close-up lens, aggregates down to 100 μm diameter could be resolved. The initial bedload was concentrated during erosion over the enclosed area in the centre of the chamber and thus the camera and the turbidity meter detected very small amounts of particles. This made this approach a very sensitive method to detect the erosion threshold since very small increments in bottom stress τ were detected and nearly immediately (time lags in the range of seconds) identified the increase in particle count or turbidity.

The particle camera technique is standard for particle observations (Eisma et al., 1996). The camera was focussed on particles in a plane 15 cm from the camera housing. Very short exposure times of 1/5000 s were required to get a satisfactory resolution with the prevailing particle velocities in the chamber. The small focal depth of approximately 5 mm prevented sizing errors, which are possible when particles are out of focus. The water volume photographed was approximately 1.9 cm^3. For back illumination, the camera was directed vertically towards a 10 W halogen bulb behind a whitened glass plate. This back illumination technique, by which particles appear dark on a light background, was used to avoid fuzzy boundaries of low-density aggregates under high flow velocities (Fennessy et al., 1994). The video pictures were transferred onto a Macintosh computer and analysed with a public-domain image analysis program (Image 1.59). Random samples of focussed, frozen video pictures were analyzed. The number of analysed pictures was chosen to provide a total sample of up to 200 sharp-edged resuspended aggregates. Per picture, a maximum of 20 individual aggregates was present. Although the focal depth was 50 times the diameter of the size of a 100 μm aggregate, these particles were not missed because the abundance of all aggregates in the small water volume measured was low. Maximum diameter of the particles was defined as the floc diameter normal to the fall trajectory. For each experiment, the taped videos were calibrated by a metric grid recorded in the laboratory at the same settings as the video pictures. The image analysis system in turn was calibrated with displays of fishing-line of 80, 200, 360 and 1000 μm diameter. Particles of 80, 163, 200, 360 and 1000 μm diameter were found to be over- or underestimated in size by up to 13, 7, 4, 8 and 5% respectively (Thomsen et al., 1996).

Data on density and kinematic viscosity of the sea water were derived from a CTD (Seabird SeaCat), which was deployed at each station during core collection. The mineralogic composition of the bottom sediments on the transects and the mineralogic composition of the eroded material (aggregates and primary particles) of the cores was determined by X-ray diffraction (Biscaye, 1965). Microscopic analysis of

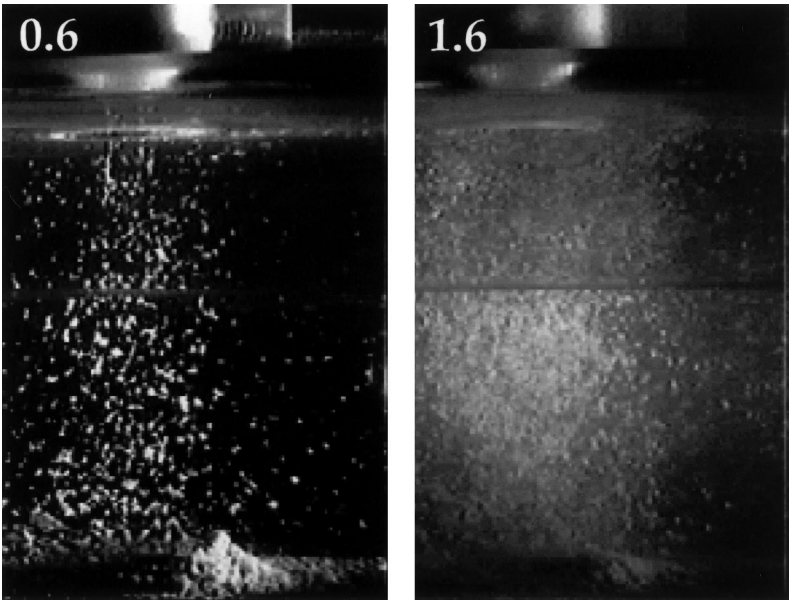

Fig. 3. Video pictures demonstrating the resuspension of continental margin sediments as different particle types under shear velocities of 0.55 and 1.61 cm s^{-1} from sediments of the Rockall Trough at 2815 m water depth. Resuspension of organic 100^{+} aggregates occurs at u_{*} of 0.55 cm s^{-1} whereas the underlying primary sediment was eroded at thresholds u_{*c} of 1.61 cm s^{-1}. Note that a transmissiometer would not see the entrained aggregated mass fraction. For better visualisation, a 90° illumination and a smaller magnification was used.

aggregates was done with a Zeiss Axiovert fluorescence microscope, with numbers of attached bacteria determined by the Acridine Orange epifluorescence direct counting technique of Hobbie et al. (1977). For analysis of both bacteria and aggregate sizes the image analysis system was used according to the method Thomsen and Ritzrau (1996). The carbon conversion factor of 0.4 pg C μm^{-3} cell volume (Bjørnsen, 1986) was used for bacterial organic carbon determinations. Mineral composition and bacterial biomass measurements were made on the same subcores as tested in the chamber. Erosion measurements were made on subcores taken from all sites. Statistics were obtained with the statistical software "Stat View II" for Macintosh computers. The settling velocities of aggregates were determined by a particle camera/settling cylinder (10 cm diameter, temperature controlled, Thomsen, 1998) for both in situ and experimentally eroded samples. From this data set we obtained a data pool which permitted us

1. to obtain thresholds, identify the structure of the bed surface,
2. to obtain details of the sedimentological and organic features of the resuspended material, and,
3. to search for a universal pattern and model of lateral sediment transport on continental margins.

3. Results

Sediments on the continental margins (212–4940 m water depth) consisted of an aggregated surface layer, which covered the underlying primary particles of cohesionless (shallower) and cohesive (deeper) type. At all transects (21 stations), core erosion in the first stage yielded aggregates >100 μm (called 100^+aggregates) at critical friction velocities (u_{*c}) of 0.44–1.16 cm s^{-1}. The erosion thresholds of underlying sediments typically increased from 0.68 to 2.05 cm s^{-1} from shallow to deeper sites, with upper-slope sediments being more sandy than the cohesive clay sediments found at deeper sections of the continental rise. Table 1 and Fig. 4 (averaged threshold data of the individual sites on each transect) summarise these results. At all stations, 100^+aggregates of the top layer appeared as the first resuspension product. They were very stable at all stations and did not disaggregate when moving through either the pump-driven recirculation path of the erosion chamber (hitherto the shear rates are undetermined in the pump head at a flow rate of 300 ml min^{-1}) or the viscous sublayer with relatively high shear rates up to 54 s^{-1} ($\delta_{viscous} = 830$ μm, $u_{*C} = 0.9$ cm s^{-1}) during the experiments. The aggregates consisted of up to 75 wt% of organic matter, which was mostly refractory with a carbon/nitrogen ratio exceeding 8, and lithogenic material ($\geqslant 25\%$) was embedded in the amorphous matrix of the organic matter. Aggregates contained remnants of faecal pellets, meiofauna organisms and shell debris of foraminifera. The mineralogical composition of the 100^+aggregates was similar to the underlying sediments. The mineral composition was similar at Vigo and Rockall with illite, kaolinite and chlorite being dominant, but chlorite was much more abundant at Rockall (36%) than at Vigo (12%). 32–71% of the bacterial mass of the BBL was particle attached and covered the organic matrix of the aggregates. Approximately 1% of the organic fraction was labile bacterial organic carbon.

In the Rockall Trough, resuspension started with the erosion of a few elongated 100^+aggregates of organic origin, up to 1 cm in length and 200 μm in diameter, termed 'stringers', followed by more abundant spherical 100^+aggregates with median diameters of 895–2403 μm under friction velocities u_* of 0.55-0.67 cm s^{-1} (see Table 1). Subsequent increase of u_* resuspended most of the 100^+aggregates 447 μm in median diameter at $0.8 < u_* < 1.17$ cm s^{-1} (Fig. 3). This pattern was common to all stations. The 100^+aggregates found at the stations of the Goban Spur, Whittard Canyon and Vigo transects showed median diameters of 224–344 μm. Aggregates of that size had a settling velocity of 0.05–0.08 cm s^{-1}, and an estimated excess density of ≈ 0.026 g cm^{-3}. The value was back calculated from Stokes Law and measured settling velocities for particles with $Re < 1$, determined in a settling column. The largest 100^+aggregates (with median diameters >2000 μm) were always resuspended first under lowest flow speeds (and thus wall shear stress). These aggregates, which were found only in May 1997 on the Rockall Trough transect, contained diatom frustules and were highly transparent.

On the continental margin, the grain size of the sediment underlying the 100^+aggregates significantly decreased with increasing water depth (Kendall's Tau $= \sim 0.6$, $p < 0.0001$). On the transect at Goban Spur, the critical friction velocity of underlying sediment increased with water depth from 0.86 to 1.80 cm s^{-1}. Between 1000 and

Table 1
Critical shear velocity measurements for different sediments at different depths collected during three cruises to the European continental margins of the Celtic Sea between 45° and 55°N, 5° and 25°W, in the months of July 1995, August 1996, May 1997, August 1997 and August 1998

Date	Station	Depth (m)	Underlying sediments				Aggregate layer at the sediment surface				Aggregates in the bottom water (10–40 cm a.b.)	
			Mean (μm size)	d_{50} (μm size)	u_{*c} (cm/s)	Nm^{-2}	Mean (μm size)	d_{50} (μm size)	u_{*c} (cm/s)	Nm^{-2}	Mean (μm size)	d_{50} (μm size)
7/95	Goban Spur	670	90	90	0.86	0.08					325 ± 120	293[a]
		1028	61	54	0.98	0.10					381 ± 190	322[a]
		1445	20	20	1.62	0.27					226 ±97	207[a]
		3660	8	6	1.80	0.34					301 ± 142	276[a]
		2150	20	18	1.35	0.19	335 ± 102	302	0.75	0.06		
5/97	Rockall	845	18	20	1.40	0.20	987 ± 607	895	0.67	0.05		
		2215	15	10	1.61	0.27	2085 ± 970	1898	0.55	0.03	2129 ± 1156	1826[a]
		2820	18	12	1.85	0.36	2768 ± 1353	2403	0.65	0.04		
		2815	25	15	1.61	0.27	2312 ± 1121	2167	0.55	0.03		
8/96	Whittard	212	95	91	0.68	0.05	528 ± 364	413	0.64	0.09	507 ± 350	392[a]
		803	34	30	1.25	0.16	406 ± 239	348	0.92	0.09	427 ± 195	396[a]
		1530	25	24	1.79	0.33	138 ± 38	125	0.98	0.10	173 ± 103	129[a]
		3711	6	5	2.05	0.44	192 ± 97	146	1.16	0.14	259 ± 148	184[a]
8/97	Vigo	2275	9	8	1.73	0.31	212 ± 54	204	0.81	0.07		
		1645	16	12	1.82	0.34	206 ± 52	203	1.13	0.13		
		1756	11	5	1.61	0.30	352 ± 124	327	1.15	0.14		
		2602	5	8	1.49	0.23	298 ± 147	264	0.92	0.09		
8/98	Vigo	879	35	20	1.05	0.11	798 ± 333	721	0.44	0.02	778 ± 468	700[a]
		2570	34	25	1.20	0.15	513 ± 69	447	1.00	0.10	479 ± 172	433[a]
		3380	12	8	1.25	0.16	435 ± 177	406	0.90	0.08	433 ± 171	412[a]
		4940	8	6	1.85	0.36	382 ± 100	361	0.90	0.09	386 ± 172	354[a]

[a]In situ particle camera data obtained with the BIOPROBE system (Thomsen et al., 1994).

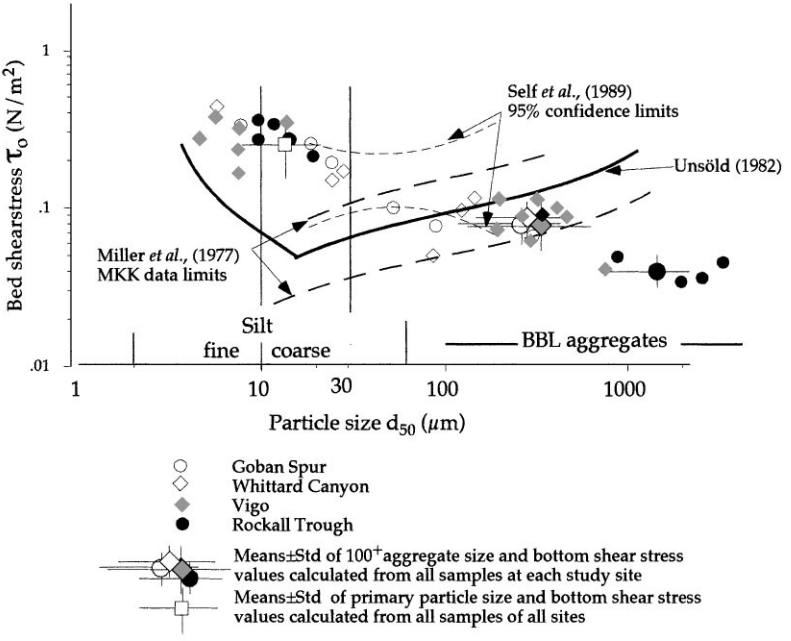

Fig. 4. Critical bed shear stress for erosion of continental margin sediments, showing the onset of a cohesion effect at about 30 μm. The black curve represents the Shields curve modified after Unsöld (1982). The wide-dashed lines refer to the uncertainty limits of available high-quality data evaluated by Miller et al. (1977), and the narrow-dashed lines those of Self et al. (1989). Larger rectangles show means ± SD of 100 + aggregate size and bottom shear stress values calculated from all samples at each study site and means ± SD of primary particle size and bottom shear stress values calculated from all samples of all sites.

1470 m, the threshold value u_{*c} of the underlying sediment increased from 0.98 to 1.62 cm s^{-1}, coinciding with a decrease in median sediment size from 54 to 20 μm and a change to clay-containing cohesive sediments. In the Whittard Canyon, u_{*c} increased from 0.68 to 2.05 cm s^{-1}, between 212 and 3711 m water depth. At Rockall Trough, u_{*c} increased from 1.40 to 1.85 cm s^{-1} from 845 to 2820 m water depth, and at the Iberian continental margin from 1.05 to 1.85 cm s^{-1} between 879 and 4940 m. At all study sites (Fig. 1), 100$^+$ aggregates were photographed in the water column at 20–40 cm above the bed with the BIOPROBE water sampler (Thomsen and van Weering, 1998. Analyses of the mean and median sizes of these in situ aggregates, shown in Table 1 (marked by a), reveals close agreement with the size of eroded aggregates from the shipborne chamber experiments ($\rho = 0.92$, $p = 0.009$, Spearman Rank). For all critical friction velocities determined, there was a negative correlation between particle size and erosion resistance (Kendall's $\tau = \sim 0.75$, $p < 0.0001$).

4. Discussion

4.1. Thresholds and types of eroded particles

One objective of measuring the critical shear velocity for incipient motion was to bring such data from continental margins into context with past studies. Our results, plotted in Fig. 4 along with the 95% confidence limits for initial particle transport of Self et al. (1989) and the threshold curve presented by Miller et al. (1977), reveal that the cores investigated in the shipborne chamber eroded at critical shear stresses comparable to the values of Self et al. (1989) for the size range of coarse silt. The silty sediments analysed in our study contained 15–40% of particles < 6.3 μm, and the onset of a cohesion effect of primary sediments started to show at about 30 μm. Thus, silt with average sizes < 30 μm behaved in the same way as clay (< 2 μm), and silt coarser than 30 μm should display size sorting behaviour. This result is different from the calculations of McCave et al. (1995), who suggested 10 μm as size discriminator between non-cohesive and cohesive sediment behaviour. Since their proposed length scale (8–11 μm) is consistent with the modified Shields diagram of Unsöld (1982), determined for quartz in seawater (Fig. 4), we propose that at the present margin sites both the higher bed shear stresses and the earlier onset of cohesion (that is, at larger diameters) compared to those proposed by McCave et al. (1995) are due to sediment stabilization by microbial exudates. The erosion threshold data were obtained in the summer, when biological activity on surface sediments is high at the study site (Duineveld et al., 1997; Pfannkuche and Soltwedel, 1998; Soetaert et al., 1996). Evidence for the importance of biological adhesion to critical stress for incipient transport has been demonstrated by various authors (Nowell et al., 1981; Parchure and Mehta, 1985; Grant and Gust, 1987; Dade et al., 1990), and Self et al. (1989) came to similar conclusions for their data on erosion resistance of cohesive sediments. Microbial exudates can increase the critical bed shear stress by a factor up to 5, and the presence of animal burrows within sediments can lead to the strengthening of the sediment bed as well (Meadows et al., 1991). The erosion chamber used in our study reliably generates desired bottom stress distributions to an accuracy that such bio-stabilization (or biodestabilization) can be resolved. However, it should be pointed out that intense surface deposit feeding can result in increased particle entrainment (Nowell et al., 1981; Thomsen and Flach, 1997) and, consequently, biodestabilization.

Statistical testing of the erosion results from all stations of all transects revealed that the particles eroded off the cores showed significantly decreasing erosion resistance with increasing particle size. In the size range 30–450 μm, both primary particles and 100^{+}aggregates from the upper slope stations at all sites showed non-cohesive behaviour (Miller et al., 1977; see Fig. 4). Here the particles fit into a Shields diagram and behaved like sand grains of appropriate size (Kineke and Sternberg, 1989).

However, both smaller- and larger-diameter particles show deviations from the classical stress versus size diagram. The primary sediment particles < 30 μm have higher thresholds, which we attribute to biological stabilisation (although reduced water contents in the core pore space cannot be ruled out either), and the particles > 450 μm show lower erosion resistance, which decreased with increasing aggregate

size. These 100^+aggregates were resuspended at critical friction velocities $0.45 < u_{*c} < 0.65\ \mathrm{cm\ s^{-1}}$ and contained primary sediment particles and solid debris, but they carried a dominant fraction of amorphous organic material (up to 75 wt%) compared to the underlying surface sediments (< 1 wt%, Lohse et al., 1998). Due to their low excess density, which through settling experiments was determined to be very close to the values predicted by McCave, (1984) for the collected 100^+aggregate size range, the non-dimensional Shields variable Θ exceeded the cohesionless-particle curve. Erosion, transport and deposition of the 100^+aggregates appears to be controlled by forces related to cohesion and stickiness in addition to gravitational and turbulence effects. This finding needs to be investigated in more detail, particularly in view of earlier conclusions by Kineke and Sternberg (1989) that BBL aggregates settling in the water column may behave like sand grains of appropriate size.

The aggregates of the 140–450 μm size range, which dominate the sinking particle pool in the BBL at the continental margin sites investigated, do not originate from recent surface production since they are refractory and contain both too little labile organic matter with mineralizable carbon and too little labile bacterial organic carbon. The mineralizable carbon of these 100^+aggregates was insufficient to change the overall high C/N ratio of > 8. From the nutrient and mineralogic analysis of their constituents, we conclude these flocs originate in the benthic zone, carried along with the flow. Along the study transects, the upper continental margin (212–1028 m water depth) defines a characteristic sedimentological zone characterized by the non-cohesive behaviour of the primary sediment particles (sandy silt). Progressing downslope to greater depths, a clear separation in threshold values and particle composition arises between the cohesive 100^+aggregates forming the top surface layer and the cohesive primary particles of the underlying sediments (Fig. 4).

4.2. The two layer concept of the sediment interface

By comparing the means $\pm$ SD values of the sizes of the 100^+aggregates and the critical friction velocity values for all samples from each study site with those of the primary particles from samples of all sites (Fig. 4), it becomes evident that a gap in critical bed shear stress exists at approximately $0.1\ \mathrm{N\ m^{-2}}$ between these two groups of particles. Particles above and below the $0.1\ \mathrm{N\ m^{-2}}$ stress discrimination value ($u_* = 1\ \mathrm{cm\ s^{-1}}$), which separates the surface aggregates from deeper cohesive particle behaviour, have a difference in u_{*c} of at least $0.2\ \mathrm{cm\ s^{-1}}$ and a mean difference of $0.6\ \mathrm{cm\ s^{-1}}$ (Fig. 4). In a steady turbulent boundary layer with a drag coefficient of 3×10^{-3}, $\tau_0 = 0.1\ \mathrm{N\ m^{-2}}$ occurs under a flow speed of $15\ \mathrm{cm\ s^{-1}}$ at 1 m above bed. A u_* range of $0.6\ \mathrm{cm\ s^{-1}}$ is equivalent to a flow speed range of $\pm 5\ \mathrm{cm\ s^{-1}}$ about this mean. We can thus distinguish between an underlying sediment layer, bound by both physico-chemical and biological adhesion forces, and a more easily resuspendable surface aggregate layer.

The concept of a two-layered bed model is not new. Krone (1962) and Partheniades (1965) have already developed a sediment erosion model for cohesive material which recognises the bed as being made up of aggregates of different order, and erosion as caused by their rupture. The presently open question however, is the extent to which

aggregates can retain their individuality when exposed to multiple, cyclic erosion–deposition events such as tides. For example, McCave et al. (1995) suggested that the hydrodynamic process of particle sorting in the viscous sublayer tends to act on particles of sizes greater than 10 μm (quarz settling velocity equivalent) such that they are increasingly likely to be separated by size and settling velocity. The (cohesionless) silt coarser than 10 μm would respond to the bottom shear stress by being sorted by size and thus could be a useful current strength indicator. Settling of seasonal or bloom-related large phytodetrital aggregates can be neglected: because of fast mineralization they do not show up in the geological record. The 100^{+}aggregates are deposited on the sea floor, and these particles are expected to accumulate on the sea floor and cover the sediment surface. Because of their low number concentrations in the benthic boundary layer (BBL), they are not able to scavenge single particles $\geqslant 10$ μm during settling by the different aggregation processes identified in the BBL (Thomsen and McCave, in press). Their strength against breakup is attributed to formation and compaction under high shear conditions associated with massive sediment erosion events such as strong benthic storms. Thus, the 100^{+}aggregates should not affect the deposition and sorting of the $\geqslant 10$ μm fraction, so the latter should consequently remain an indicator of current strength (McCave et al., 1995) independent of aggregate transport processes in the BBL. Since, they are generated during high-energy events, they should retain their individuality even under multiple cyclic erosion-deposition events. Disaggregation and loss of individuality is expected only under shear conditions exceeding those during build up.

4.3. *The resuspension, transport, deposition loop*

At the individual study sites, the BBL aggregates in the 140–450 μm size range, which dominate the 100^{+}aggregates with mean values from 308 ± 151 to 383 ± 211 μm and median values from 224 to 344 μm, form the top layer of the sea floor and are resuspended at mean thresholds of u_{*c} of 0.8–0.9 cm s^{-1}. This is comparable to particles of similar size but much higher density and settling velocity (i.e. sand). The less abundant aggregates > 450 μm in diameter were resuspended at critical friction velocities 0.45–0.65 cm s^{-1}. The values of u_{*c} translate for a logarithmic layer into velocities u_{100} (at 1 m height) of 9–23 cm s^{-1}. Once suspended, the aggregates are transported over much greater distances because of their low settling velocities of 0.06 ± 0.02 cm s^{-1} compared to sand of similar size but up to two order of magnitude higher settling velocities. In combination with the thresholds (and entrainment rates) of the resuspended material, the local flow field determines the ensuing transport pattern. Steep slopes like the Whittard Canyon site and the continental margin off Vigo result in locally steeper isopycnical gradients and faster mean flow conditions (Huthnance, 1995). At the Celtic Sea continental margin, bottom flow velocities $u_{100} > 15$ cm s^{-1} (taken as mean critical threshold velocity to resuspend the top-layer aggregates) occur and are directed downslope (Pingree and LeCann, 1989; van Weering et al., 1998). Spot measurements at 10–50 cm a.b. of vertical mean flow profiles at different times of the year at the different study sites revealed shear velocities (derived from the velocity data via the law of the wall) ranging from

0.2–2.0 cm s^{-1} (Thomsen and van Weering, 1998). Internal tides on the continental margin provide additional driving forces to push local currents beyond critical erosion conditions. For example, at Porcupine Bank, internal tides control the resuspension of bottom material at 1800–2800 m water depth (Dickson and McCave, 1986), with currents exceeding 15 cm s^{-1} for 1.8–4.1% of the time (Thorpe and White, 1988). For the Celtic Sea, tidal bottom currents exceeding 15–20 cm s^{-1} were found on the continental margin at 1500 m water depth in late summer and winter with a net downslope transport 25% of the time (van Weering et al., 1998). These flow conditions are typical for our study sites and are high enough to resuspend the total surface layer of aggregates (during at least one phase of the tidal cycle) but not the underlying sediments. Once resuspended, these BBL aggregates are transported in flow direction over long distances while being lifted or settling depending on the particulars of the tide-modulated flow field. The details of this transport loop concept require further combined sedimentological–hydrodynamical experiments in situ concurrent with ship-borne simulations on recovered cores for which the erosion device can be programmed as a tide-simulating erosion/deposition chamber.

For the erosion of the primary cohesive sediments underlying the BBL aggregates, flow conditions able to generate $\tau_c > 0.14$ N m^{-2} ($u_* > 1.2$ cm s^{-1}) are needed. Extreme events such as benthic storms can produce these flow velocities in excess of 25 cm s^{-1}, as reported for the deep sea by Hollister and McCave (1984) and Gross et al. (1988). To erode mid-slope continental margin sediments at Goban Spur, where $u_{*c} > 0.25$ N m^{-2} ($u_* > 1.6$ cm s^{-1}), flow speeds $u_{100} > 45$ cm s^{-1} are needed to initiate sediment transport. Besides a biologically mediated increase of threshold, another reason for this high local threshold value is the relatively frequent occurrence of strong bottom currents during autumn and winter, during which flow velocities $u_{40} > 30$ cm s^{-1} leave an extremely stable primary sediment surface (Thomsen and van Weering, 1998).

The 100^+ aggregates carry a carbon signature proposed as "Ocean background value" (Thomsen, 1998). Of this carbon, only 1–1.3 wt% is fresh bacterial organic carbon, which is accessible to the benthic community during the whole year. Thomsen (1998) further suggested that under the flow conditions found at the continental margins, massive particle flux occurs during the tidal cycles and consequently food limitation should rarely occur for mid- and lower-slope deposit feeders since these animals live between horizontal drifting BBL aggregates. It will thus be important to extend the currently used erosion chambers into multiple-cycle erosion/deposition chambers simulating actual bottom stress pattern of the in situ sites this way the bioavailabilty of aggregate-related food over the full aggregate size spectrum would become detectable and it would become obvious that the oxygen exposure times of particles in the BBL are responsible for the carbon burial rate at continental margins.

Acknowledgements

The authors wish to thank the crews of RV *Pelagia* and RV *Meteor* for technical assistance during the cruises. Jens Greinert kindly provided data on aggregate

mineralogy. This study was funded by the European Union during the MAST II OMEX program (MAS3-CT97-0076).

References

Auffret, G.A., Khripounoff, A., Vangriesheim, A., 1994. Rapid post-bloom resuspension in the Northeastern Atlantic. Deep Sea Research 41, 925–939.

Biscaye, P.E., 1965. Mineralogy and sedimentation of recent deep-sea clay in the Atlantic Ocean and adjacent seas and oceans. Geological Society of American Bulletin 76, 803–832.

Biscaye, P.E., Flagg, C.N., Falkowski, P.G., 1994. The shelf edge exchange processes experiment, SEEP-II: an introduction to hypotheses, results and conclusions. Deep-Sea Research II 41, 231–253.

Bjørnsen, P.K., 1986. Automatic determination of bacterioplankton biomass by image analysis. Applied Environmental Microbiology 51 (6), 1199–1204.

Blaume, F., 1992. Hochakkumulationsgebiete am norwegischen Kontinentalhang. Ber. SFB 313, 36 Kiel University, ISSN 0942-119X

Booij, K., Sundby, B., Helder, W., 1994. Measuring flux of oxygen to a muddy sediment with a cylindrical microcosm. Netherlands Journal of Sea Research 31 (1), 1–11.

Buchholtz-ten Brink, M.R., Gust, G., Chavis, D., 1989. Calibration and performance of a stirred benthic chamber. Deep Sea Research 36, 1082–1101.

Dade, B., Davis, J.D., Nichols, P.D., Nowell, A.R.M., Thistle, D., Trexler, M.B., White, D.C., 1990. Effects of bacterial exopolymer adhesion on the entrainment of sand. Geomicrobiological Journal 8, 1–16.

Dickson, R.R., McCave, I.N., 1986. Nepheloid layers on the continental slope west of Porcupine Bank. Deep Sea Research 33, 791–818.

Duineveld, G.C.A., Lavaleye, M.S.S., Berghuis, E.M., de Wilde, P.A.W.J., van der Weele, J., Kok, A., Batten, S.D., De Leeuw, J.W., 1997. Patterns of benthic fauna and benthic respiration on the Celtic continental margin in relation to the distribution of phytodetritus. Internationale Revue gesamten Hydrobiologia 82, 395–424.

Eisma, D., Dyer, K.R., v. Leussen, W., 1996. In situ determination of settling velocities of suspended fine grained sediments — a review. Journal Sea Research 36 (1/2), 156.

Fennessy, M.J., Dyer, K.R., Huntley, D.A., 1994. INSSEV: an instrument to measure the size and settling velocity of flocs in situ. Marine Geology 117, 107–117.

Graf, G., Gerlach, S.A., Linke, P., Queisser, W., Scheltz, A., Thomsen, L., Witte, U., 1995. Benthic–Pelagic coupling in the Greenland–Norwegian Sea and its effects on the geological record. Geologische Rundschau 84, 49–58.

Grant, J., Gust, G., 1987. Prediction of coastal sediment stability from phytopigment content of purple sulfur bacterial mats. Nature 330, 244–246.

Gross, T.F., Williams, A.J., Nowell, A.R.M., 1988. A deep sea sediment transport storm. Deep Sea Research 331, 518–521.

Gust, G., 1988. Skin friction probes for field applications. Journal of Geophysical Research 93, 14121–14132.

Gust, G., Müller, V., 1997. Interfacial hydrodynamics and entrainment functions of currently used erosion devices. In: Burt, N., Parker, R., Watts, J. (Eds.), Cohesive Sediments. Wiley, Chichester, UK, pp. 149–174.

Hobbie J.E., Daley, R.J., Jasper, S., 1977. Use of Nucleopore filters for counting bacteria by fluorescence microscopy. Applied and Environmental Microbiology 33, 1225–1228.

Hollister, C.D., McCave, I.N., 1984. Sedimentation under deep-sea storms. Nature 309, 220–225.

Huthnance, J.M., 1995. Circulation exchange and watermasses at the ocean margin: the role of physical processes at the shelf edge. Progress in Oceanography 35, 353–431.

Jahnke, R.A., Reimers, C.E., Craven, D.B., 1990. Intensification of recycling of organic matter at the sea floor near the ocean margins. Nature 348, 50–54.

Kineke, G.C., Sternberg, R.W., 1989. The effect of particle settling velocity on computed suspended sediment concentration profiles. Marine Geology 90, 159–174.

Krone, R.B., 1962. Flume studies of the transport of sediments in estuarial shoaling processes. Hydraulic Engeneering and Sanitary. Engineering Research Laboratory University of Califonina, Berkeley, 110 pp.

Lohse, L., Helder, W., Epping, E.H.G., Balzer, W., 1998. Recycling of biogenic debris along a shelf slope transect in the northeastern Atlantic (Goban Spur). Progress in Oceanography 42, 77–111.

McCave, I.N., 1984. Size spectra and aggregation of suspended particles in the deep ocean. Deep Sea Research 31, 329–352.

McCave, I.N., 1986. Local and global aspects of the bottom nepheloid layers in the world ocean. Netherlands Journal of Sea Research 20, 167–181.

McCave, I.N., Manighetti, B., Robinson, S.G., 1995. Sortable silt and fine sediment size/composition slicing: parameters for palaeocurrent speed and palaeoceanography. Paleoceanography 10 (3), 593–610.

Meadows, P.S., Tait, J., Hussain, S.A., 1991. Effects of estuarine infauna on sediment stability and particle sedimentation. Hydrobiologia 190, 263–266.

Middleton, G.V., Southard, J.B., 1984. Mechanics of Sediment Movement. S.E.P.M. Short Course No. 3, 2nd Edition. Tulsa, 787 pp.

Miller, M.C., McCave, I.N., Komer, P.D., 1977. Threshold of sediment motion under unidirectional currents. Sedimentology 24, 507–527.

Nowell, A.R.M., Jumars, P.A., Ekman, S.R., 1981. Effects of biological activity on the entrainment of marine sediments. Marine Geology 42, 133–193.

Opdyke, B.N., Gust, G., Ledwell, J.R., 1987. Mass transfer from smooth alabaster surfaces in turbulent flows. Geopysical Research Letters 14, 1131–1134.

Parchure, T.M., Mehta, A.J., 1985. Erosion of soft cohesive sediment deposits. Journal of Hydraulic Engineering. 111 (10), 1308–1326.

Partheniades, E., 1965. Erosion and deposition of cohesive soils. Journal Hydraulic Division American Society of Civil Engineers 91, 105–139.

Pfannkuche, O., Soltwedel, T., 1998. Small benthic size classes along the western European continental margin. Progress in Oceanography 42, 189–209.

Pingree, R.D., LeCann, B., 1989. Celtic and Armorican slope and shelf Residual currents. Progress in Oceanography 23 (4), 303–339.

Priede, M., 1999. ALIPOR (Autonomous Lander Instrument Packages for Oceanographic Research): Final Report, EU no. MAS3-CT950010

Ritzrau, W., 1996. Microbial activity in the Benthic Boundary Layer: small scale distribution and ist relationship to the hydrodynamic regime. Journal of Sea Research 36 (3/4), 171–180.

Self, R.F.L., Nowell, A.R.M., Jumars, P.A., 1989. Factors controlling critical shears for deposition and erosion of individual grains. Marine Geology 86, 181–199.

Soetaert, K., Herman, P.J.M., Middelburg, J.M., Heip, C., de Stigter, H., van v. Weering, T.C.E., Epping, E., Helder, W., 1996. Modeling 210Pb-derived mixing activity in ocean margin sediments: diffusive versus nonlocal mixing. Journal of Marine Research 54, 1207–1227.

Thomsen, L., Graf, G., Martens, V., Steen, E., 1994. An instrument for sampling water from the benthic boundary layer. Continental Shelf Research 14, No. 7/8, 871–882.

Thomsen, L., Graf, G., Juterzenka, K.v., Witte, U., 1995. An in situ experiment to investigate the depletion of seston above a suspension feeder field on the continental slope of the western Barents Sea. Marine Ecology Progress Series 123, 295–300.

Thomsen, L., Ritzrau, W., 1996. Aggregate studies in the benthic boundary layer at a continental margin. Journal of Sea Research 36, 143–146.

Thomsen, L., Jähmlich, S., Graf, G., Friedrichs, M., Springer, B., Wanner, S., 1996. An instrument for aggregate studies in the benthic boundary layer. Marine Geology 135, 153–157.

Thomsen, L., Flach, E., 1997. Mesocosm observations of fluxes of particulate matter within the benthic boundary layer. Journal of Sea Research 37, 67–79.

Thomsen, L., v. Weering, T.C., 1998. Spatial and temporal variability of particulate matter in the benthic boundary layer at the North East Atlantic Continental Margin (Goban Spur). Progress in Oceanography 42, 61–76.

Thomsen, L., 1998. Processes in the Benthic Boundary Layer at continental margins and their implication for the benthic carbon cycle. Journal of Sea Research 41, 73–83.

Thomsen, L., McCave, I.N., Aggregation processes in the Benthic Boundary Layer at the Celtic Sea Continental Margin. Deep Sea Research, in press.

Thorpe, R.S., White, M., 1988. A deep intermediate nepheloid layer. Deep Sea Research 35, 1665–1671.

Tsai, C.H., Lick, W., 1986. A portable device for measuring sediment resuspension. Journal of Great Lake Research 12 (4), 314–321.

Unsöld, G., 1982. Der Transportbeginn rolligen Material in gleichförmigen turbulenten Strömungen. Ph.D. Dissertation, Kiel-University, 145 pp.

v.Weering, T.C.E., McCave, I.N., De Stigter, H.C., Hall, I., Thomsen, L., 1998. Recent sediments, sediment accumulation, and carbon burial at Goban Spur, NE Atlantic continental margin, Progress in Oceanography 42, 5–37.

Walsh, J.J., Rowe, G.T., Iverson, R.L., McRoy, C.P., 1981. Biological export of shelf carbon: a neglected sink of the global CO_2 cycle. Nature 291, 196–201.

Wiltshire, K.H., Tolhurst, T., Paterson, D.M., Davidson, I., Gust, G., 1997. Pigment fingerprints as markers of erosion and changes in cohesive sediment surface properties in simulated and natural erosion events. In: Black, K.S., Paterson, D.M., Cramp, A. (Eds.), Sedimentary Processes in the Intertidal Zone, Vol. 139. Geological Society, (Special Publications), London, pp. 99–114.